Global mineral dust simulations with ECHAM6-HAMMOZ for modern and last glacial maximum climate conditions

S. Krätschmer[1], M. Werner[1], F. Lamy[1], C. Völker[1], M. van der Does[1]

[1]Alfred Wegener Institute, Helmholtz Centre for Polar and Marine Research, Bremerhaven, Germany

Corresponding author: Stephan Krätschmer, stephan.kraetschmer@awi.de

Stephan Krätschmer
https://doi.org/10.5194/egusphere-egu2020-5463
EGU General Assembly 2020

1. Introduction

- Ice core and marine sediment data indicate more dust deposition during glacials [1,2] (see Fig. 1 [3])
- Increased dust emissions could have been caused by extented drylands due to a lower sea level, less precipitation, less vegetation and stronger winds [4]
- Models tend to underestimate the 3- to 5-fold increase in dust depostion [2,5] by a factor of 3
- **Our study (AWI project *DustIron*, see appendix) aims to reduce data-model discrepancy by using the novel model setup ECHAM6-HAMMOZ to simulate the dust cycle for modern and Last Glacial Maximum (LGM) climate conditions**

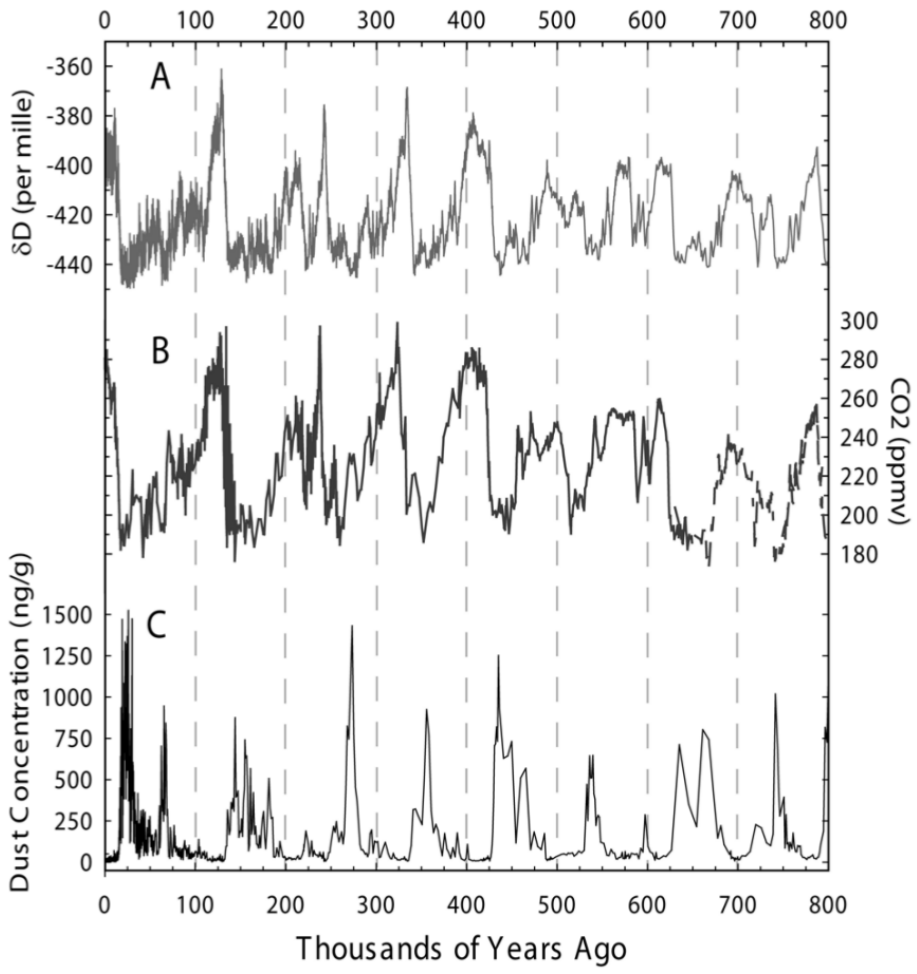

Fig. 1: Data retrieved from EDC ice core (taken from Kohfeld et al., 2009).

Stephan Krätschmer
https://doi.org/10.5194/egusphere-egu2020-5463
EGU General Assembly 2020

2. Model Setup

- We use a specific branch of ECHAM6-HAMMOZ, consisting of the general circulation atmospheric model ECHAM6, the aerosol model HAM and the atmospheric chemistry model MOZ [6] (see appendix for detailed description)
- Our setup consists of ECHAM6.1-HAM2.1 as described by Stanelle et al. (2014)
- Dust emissions are directly coupled to the land surface model JSBACH being part of ECHAM6, enabling to calculate the dust emission fluxes online from spatio-temporally varying areas due to dynamic vegetation
- Forcing data for sea surface temperature and sea ice concentration are climatological means (1979-2008 for present day, 1870-1899 for pre-industrial) from the AMIP dataset.[8] For the LGM, we use the according reconstructions from the GLAMAP dataset [9]
- LGM runs are initialised according to the PMIP4 experimental design [10]

3. Results

3.1 Overview

Model / Simulation Period / Author	Emission ($Tg\ a^{-1}$)	Burden (Tg)	Wet Dep. ($Tg\ a^{-1}$)	Dry Dep. ($Tg\ a^{-1}$)	Sedi. ($Tg\ a^{-1}$)
ECHAM6.1-HAM2.1 year 2000 (present day, PD)	1358	20	764	106	496
ECHAM6.1-HAM2.1 decadal mean 1860 – 1869 (pre-industrial, PI)	847	15	508	49	298
AEROCOM median, year 2000 (range) Huneeus et al. (2011)	1123 (514 - 4313)	15.8 (6.8 - 29.5)	357 (295 - 1382)	396 (37 - 2791)	314 (22 - 2475)
ECHAM6.1-HAM2.1 decadal mean LGM 21kya	5225	99	3120	528	1587
CESM, LGM 21kya Albani et al. (2019)	6272	37	-	-	-

Table 1: Key values characterising the strength of the dust cycle for PD, PI and LGM climate conditions. Additionally, results from the global dust model intercomparison in AEROCOM phase I (medians from 15 different models) [11] and CESM [12] are shown for a better comparability of our simulation results.

3.2 Simulated annual dust emission and deposition for the LGM

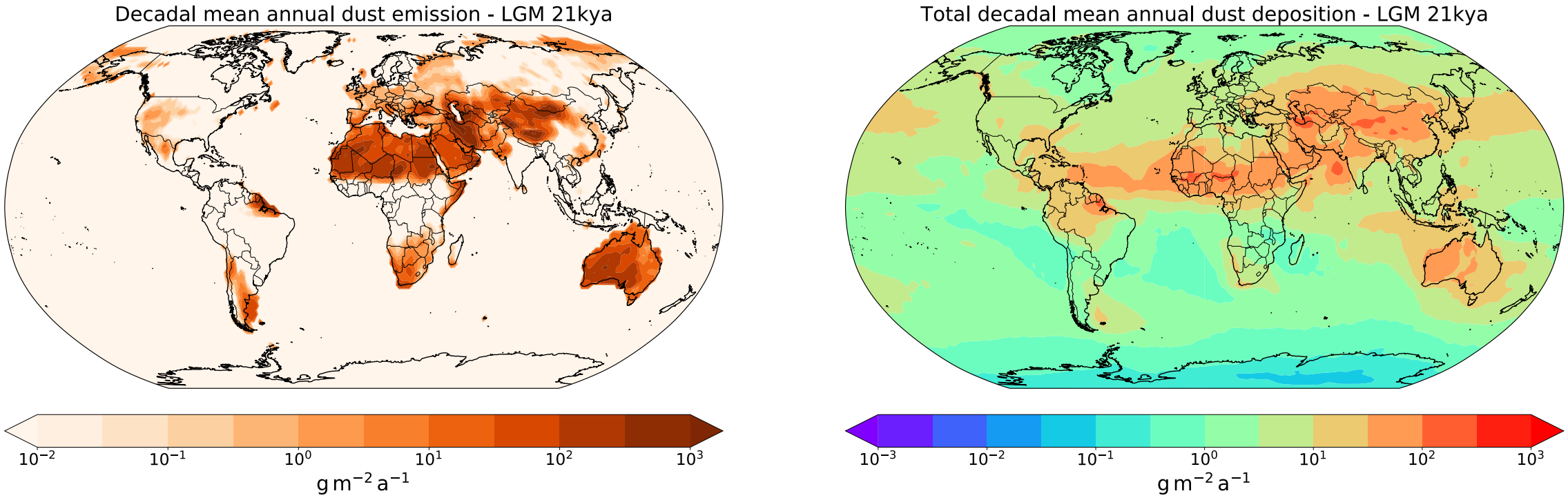

Fig. 2: 10-year means of the annual dust emission and deposition for LGM climate conditions. Dust emission seems to occur in sea areas due to the lower sea level while the coastlines show present-day conditions. The total dust deposition consists of dry and wet deposition as well as sedimentation (see Fig. 4 & 5 in the appendix).

Stephan Krätschmer
https://doi.org/10.5194/egusphere-egu2020-5463
EGU General Assembly 2020

3.3 Simulated annual dust load for the LGM

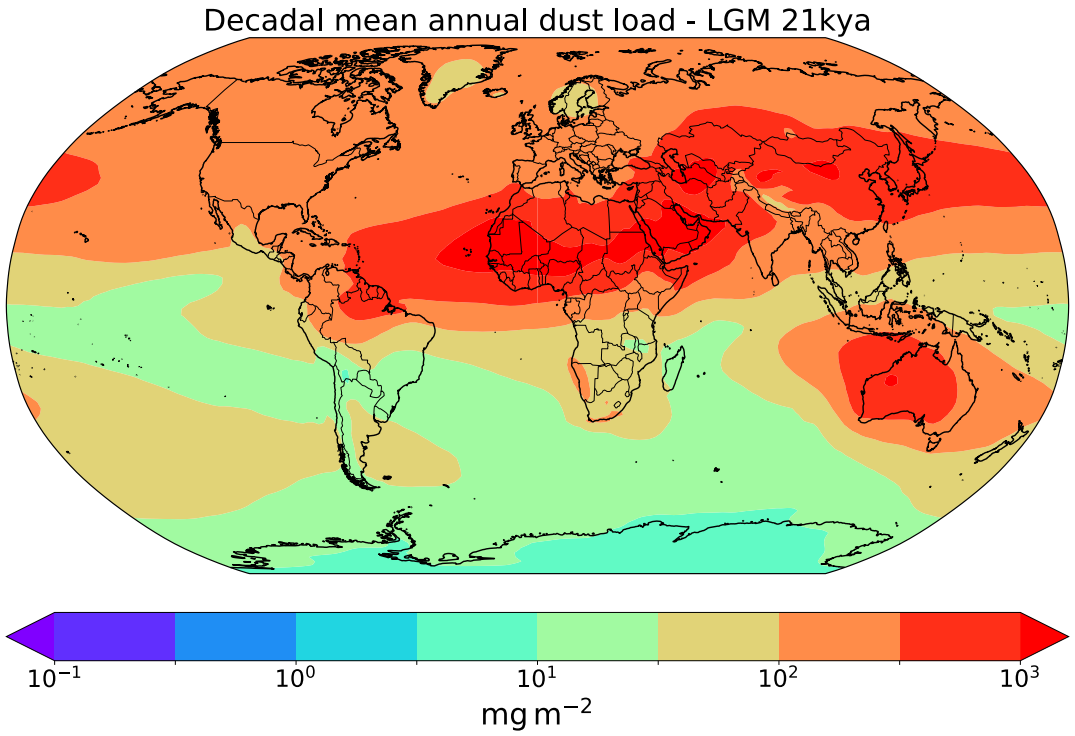

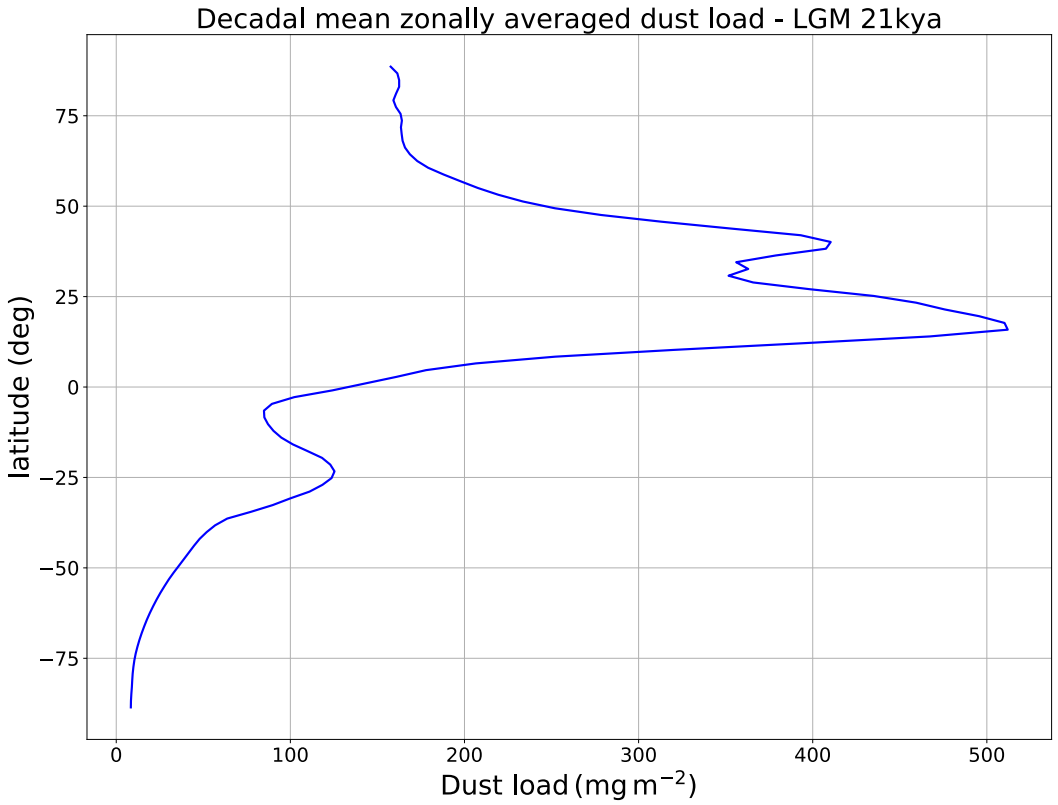

Fig. 3: 10-year mean of the annual dust load for LGM climate conditions. On the right-handed side, the zonally-averaged dust load depending on the latitude is shown.

4. Discussion

- According to Table 1, we can conclude that our setup yields results within the range of other model output
- Our results suggest a 60% increase in the strength of dust emissions from pre-industrial to present day
- The model simulates a 3.8-fold increase in dust emissions and depositions at the LGM compared to present day
- The dust emissions especially in the high northern latitudes (see Fig. 2) require further analysis since these regions were expected to be covered by vegetation
- Our next steps include in particular a detailed analysis of the contributions from different dust sources in the southern hemisphere (Patagonia, South Africa, Australia) to the total dust deposition in the Southern Ocean during the LGM

References

[1] Lambert et al.: *Dust-climate couplings over the past 800,000 years from the EPICA Dome C ice core*. Nature, Vol. 452 (2008).

[2] Lamy et al.: *Increased Dust Deposition in the Pacific Southern Ocean During Glacial Periods*. Science, Vol. 343 (2014).

[3] Kohfeld & Ridgwell: *Glacial-interglacial variability in atmospheric CO_2*. Geophys. Res. Ser., Vol. 187 (2009).

[4] Lunt & Valdes: *Dust deposition and provenance at the Last GlacialMaximum and present day*. Geophys. Res. Lett., Vol. 29, No. 22, 2085 (2002).

[5] Martinez-Garcia et al.: *Links between iron supply, marine productivity, sea surface temperature, and CO_2 over the last 1.1 Ma*. Paleoceanography, Vol. 24 (2009).

[6] Schultz et al.: *The chemistry-climate model ECHAM6.3-HAM2.3-MOZ1.0*. Geosci. Model Dev., 11, 1695-1723 (2018).

[7] Stanelle et al.: *Anthropogenically induced changes in twentieth century mineral dust burden and the associated impact on radiative forcing.* J. Geophys. Res. Atmos., 119, 13,526-13,546 (2014).

[8] Gates et al.: *An Overview of the Results of the Atmospheric Model Intercomparison Project (AMIP I)*. B. Am. Metorol. Soc., Vol. 80, No. 1 (1999).

[9] Paul & Schäfer-Neth: *Modeling the water masses of the Atlantic Ocean at the Last Glacial Maximum*. Paleoceanography, Vol. 18, No. 3 (2003).

[10] Kageyama et al.: *The PMIP4 contribution to CMIP6 – Part 4: Scientific objectives and experimental design of the PMIP4-CMIP6 Last Glacial Maximum experiments and PMIP4 sensitivity experiments*. Geosci. Model Dev., 10, 4035-4055 (2017).

[11] Huneeus et al.: *Global dust model intercomparison in AeroCom phase I*. Atmos. Chem. Phys., 11, 7781-7816 (2011).

[12] Albani & Mahowald: *Paleodust Insights into Dust Impacts on Climate*. J. Climate, Vol. 32 (2019).

[13] Stevens et al.: *Atmospheric component of the MPI-M Earth System Model: ECHAM6*. J. Adv. Model. Earth Syst., 5, 146-172 (2013).

[14] Reick et al.: *Representation of natural and anthropogenic land cover change in MPI-ESM*. J. Adv. Model. Earth Syst, 5, 459-482 (2013).

[15] Tegen et al.: *The global aerosol-climate model ECHAM6.3-HAM2.3 – Part 1: Aerosol evaluation*. Geosci. Model Dev., 12, 1643-1677 (2019).

[16] Tegen et al.: *Impact of vegetation and preferential source areas on global dust aerosol: Results from a model study*. J. Geophys. Res., 107(D21), 4576 (2002).

[17] Martinez-Garcia & Winckler: *Iron fertilization in the glacial ocean*. PAGES, Vol. 22, No. 2 (2014).

[18] Martin: *Glacial-Interglacial CO_2 Change: The Iron Hypothesis.* Paleoceanography, Vol. 5, No. 1 (1990).

Additional Slides

Further Results from the LGM Simulation

Simulated annual dry and wet dust deposition for the LGM

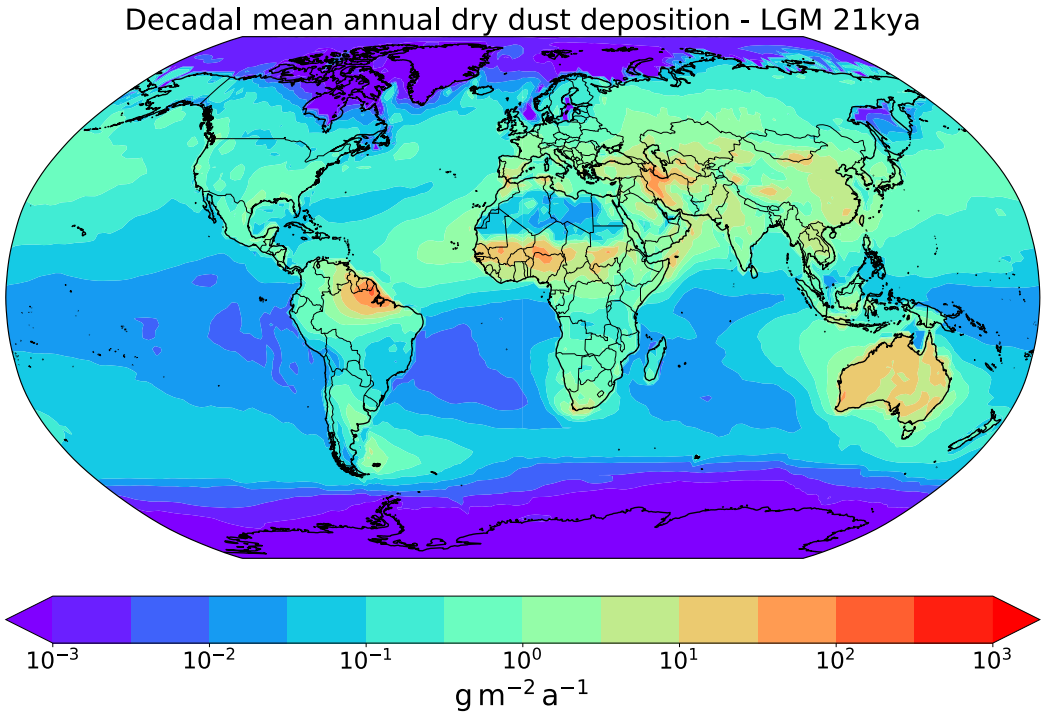

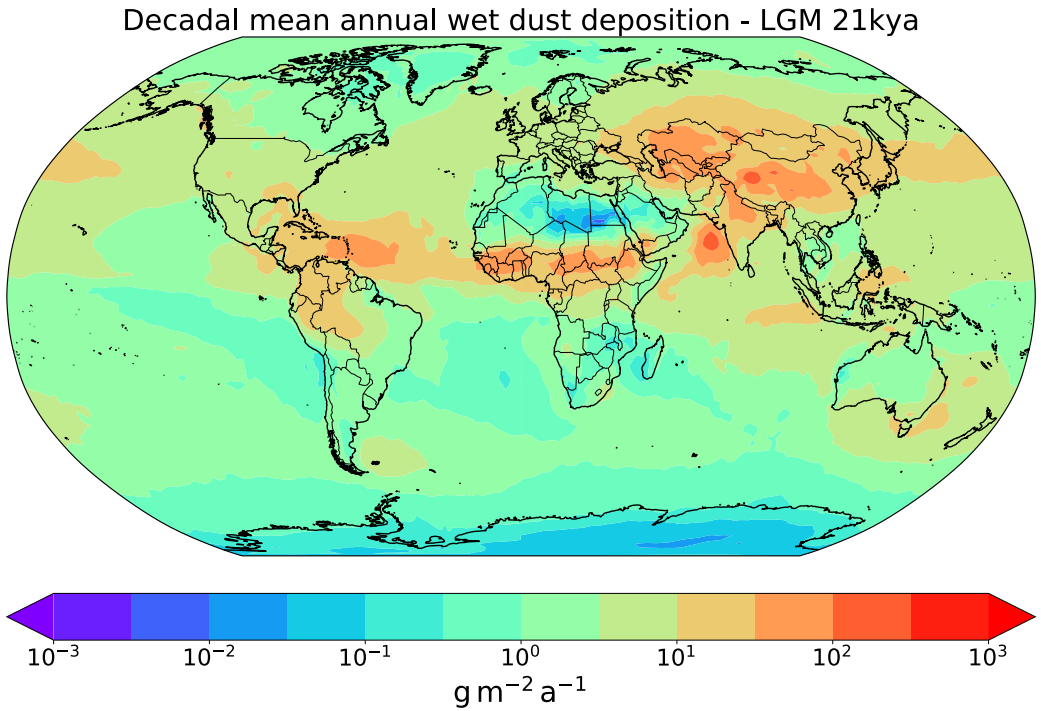

Fig. 4: 10-year mean of the annual dry and wet dust deposition for LGM climate conditions.

Simulated annual dust sedimentation for the LGM

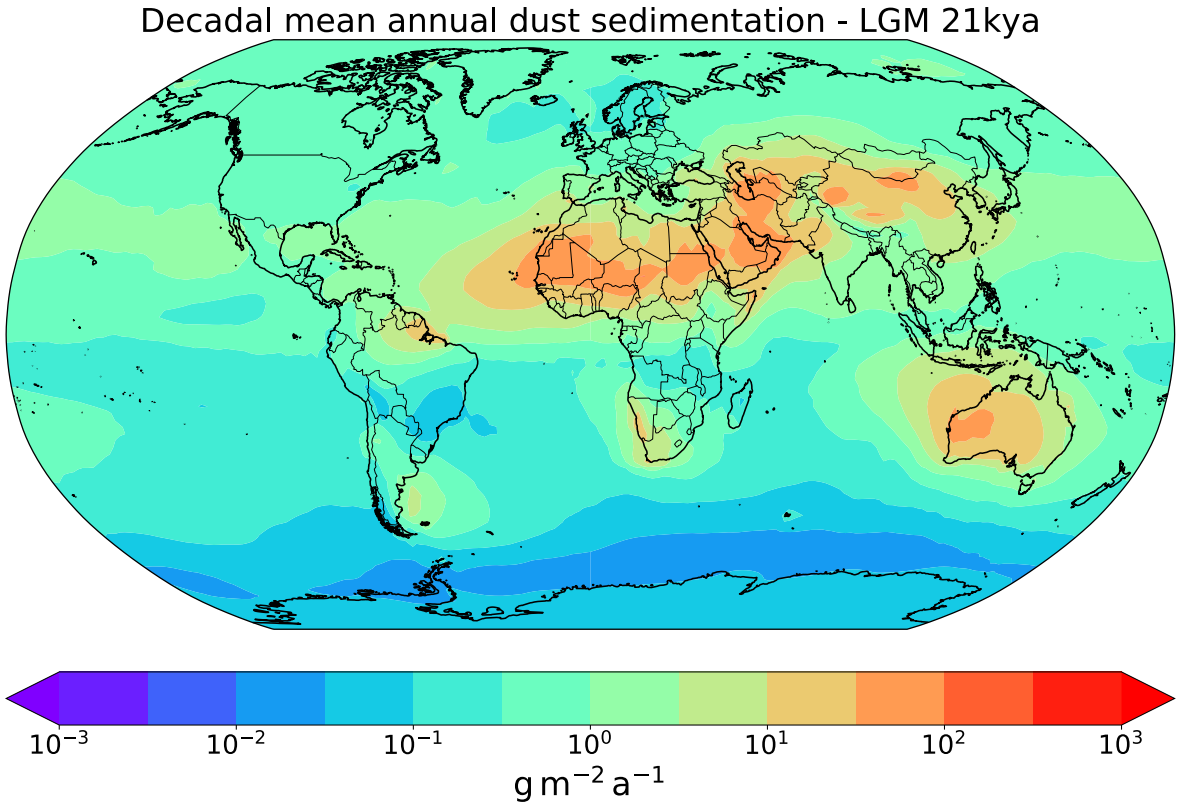

Fig. 5: 10-year mean of the annual dust sedimentation (i.e. gravitational settling) for LGM climate conditions.

ECHAM6-HAMMOZ: Overview

The main model branch ECHAM6.3-HAM2.3-MOZ1.0 consists of the latest release of the atmospheric general circulation model ECHAM6 coupled to the aerosol model HAM and the atmospheric chemistry model MOZ and is described in detail by Schultz et al. (2018). The submodules HAM and MOZ both can be switched on and off independently.

ECHAM6 uses a spectral approach to solve the prognostic equations for vorticity, divergence, temperature and surface pressure, while using a sigma-pressure coordinate on a Lorenz grid for the vertical discretization. Diabatic subgrid-scale processes, e.g. gravity waves, convection, turbulence etc., are described by parametrisations on a gaussian grid.[13] Additionally, the land surface model JSBACH is an integral part of ECHAM6. It computes dynamically the respective proportion of bare and vegetated soil surfaces, taking into account several different plant functional types.[14]

HAM uses information from ECHAM6 (e.g. wind speed) to calculate online the emission of primary aerosols (mineral dust, sea salt, black carbon etc.) and uses datasets for the emission of aerosol precursor from different sectors by using either a modal (M7) or a bin scheme (SALSA).[15] For mineral dust, three log-normal modes are used to describe the size distribution ranging from 0.2 to 1300 µm in diameter. In the standard model setup, dust emissions occur solely in potential dust source areas prescribed by an external file derived by Tegen et al. (2002) based on a combination of model output and satellite data. If the dust emission is directly coupled to JSBACH, the following factors are essentially considered: Areas covered by low-stature vegetation (e.g. grassland, tundra, shrubs etc.) are potential dust source areas. Areas covered by trees or snow, respectively, gaps sourrounded by forests cannot emit dust.[7]

The submodule MOZ computes online over 700 reactions for over 200 different atmospheric trace gases, including radical-radical reactions, oxidation chains of volatile organic components and several photolysis reactions.[6]

The Project *DustIron*

The Southern Ocean (SO) is considered to be the largest high nutrient-low chlorophyll region in the world, i.e. it is enriched in nutrients required for phytoplankton growth, however, without showing the expected blooms.[17] Martin (1990) proposed the so-called **iron hypothesis** as an explanation:

Soluble iron provided by mineral dust is the limiting factor for phytoplankton productivity in the SO. Increased dust/iron fluxes to the SO during the Last Glacial Maximum caused phytophlankton blooms and the subsequent enhanced bioproductivity contributed significantly to the decrease of the atmospheric CO_2 level from 280 ppm during interglacials to well below 200 ppm during the LGM.

Several data recently retrieved from antarctic ice cores and marine sediments from key locations in the SO strongly support the correlations suggested by the iron hypothesis for the last 800 kyr (see Fig. 1 & 6). The AWI project *DustIron* is intended to improve our understanding of those interconnections on glacial/interglacial timescales by a coupled model-data approach.

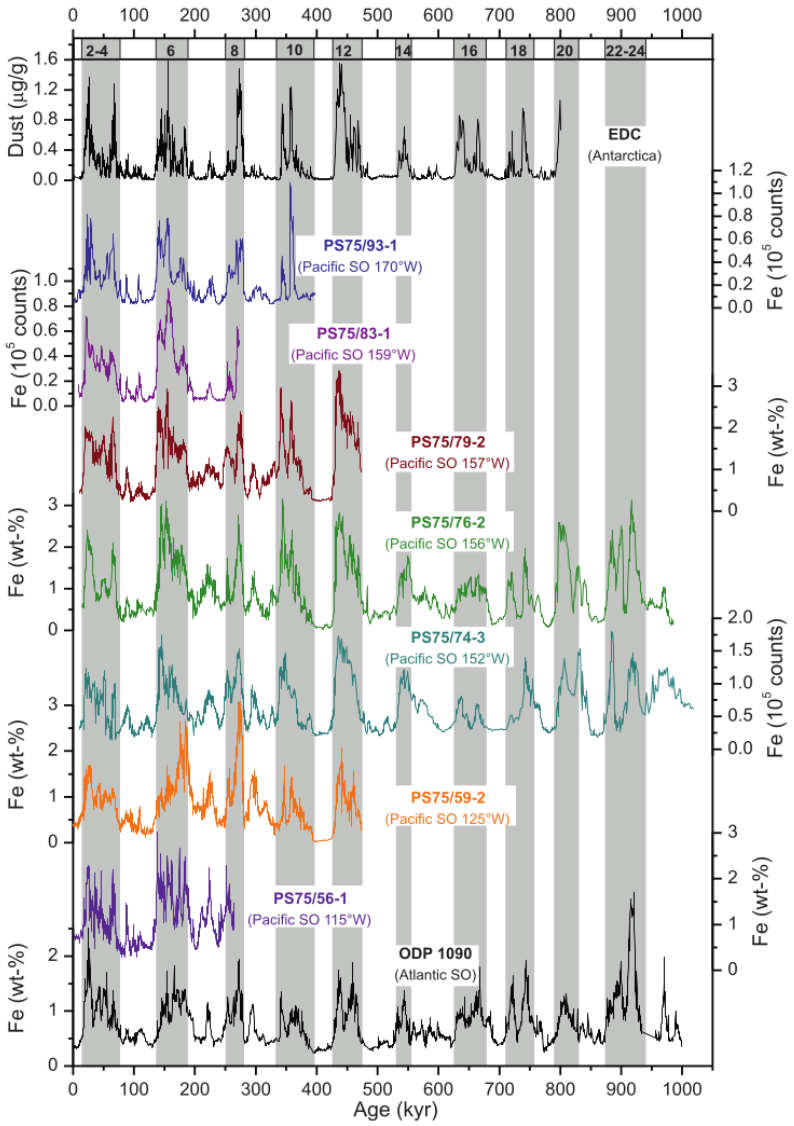

Fig. 6: Taken from Lamy et al. (2014).